Engineering Structures 151 (2017) 568–583

Contents lists available at ScienceDirect

Engineering Structures

journal homepage: www.elsevier.com/locate/engstruct

Numerical studies on the seismic responses of bridge structures with precast segmental columns

Lufeng Zhao [a,b], Kaiming Bi [b], Hong Hao [b], Xiaozhen Li [a,*]

[a] Department of Bridge Engineering, Southwest Jiaotong University, Chengdu, China
[b] Center for Infrastructure Monitoring and Protection, School of Civil and Mechanical Engineering, Curtin University, Kent Street, Bentley, WA 6102, Australia

ARTICLE INFO

Article history:
Received 6 April 2017
Revised 5 July 2017
Accepted 11 August 2017

Keywords:
Bridge structures
Segmental column
Monolithic column
Seismic response
Pounding

ABSTRACT

Recently, extensive experimental and numerical studies have been carried out to understand the seismic behaviors of segmental columns. Very limited studies, however, focused on the seismic performances of a whole bridge system with precast segmental columns. This paper carries out numerical studies on the seismic responses of bridge structures with precast segmental columns. For comparison, the seismic responses of the bridge with conventional monolithic columns are also calculated. The two-dimensional (2 D) finite element (FE) models of these two bridge types are developed by using the FE code OpenSEES. The segmental column and monolithic column are simulated by the simplified lumped-mass model and fiber-based model respectively and validated by the previous experimental studies. The calibrated column models are then incorporated into the whole bridge structures to calculate the structural responses. The influences of pounding, frequency ratio and gap size on the structural responses are investigated and discussed. Numerical results show that the bridges supported by the segmental columns or monolithic columns have very different seismic responses.

1. Introduction

To achieve the accelerated bridge construction (ABC), precast segmental columns are more and more widely used in engineering applications recently. Comparing with the conventional cast-in-place monolithic columns, precast segmental bridge columns have many obvious advantages such as the high quality control of fabrication, minimum environmental impact and smaller residual displacement after a severe earthquake [1,2]. Despite these apparent advantages, the constructions of bridges with segmental columns were normally limited in low seismic intensity regions. The application of this bridge type in regions with high seismicity is rare due to the lack of understanding on their seismic performances.

Recently extensive research works have been carried out to investigate the seismic behaviors of precast segmental columns. Hewes and Priestley [3] conducted analytical and experimental investigations on the seismic performances of unbonded post-tensioned precast concrete segmental columns with high and low aspect ratios. It was found that unbonded pre-stressed segmental columns could effectively resist the lateral earthquake loading. However, limited energy was dissipated by the segmental columns. To improve the energy dissipation capability of segmental columns, many different energy dissipation devices have been proposed by different researchers. Chang et al. [4] and Ou et al. [5] advocated the use of continuous mild steel bars, which are also named as ED bars, along the pier segments to improve the energy dissipation capacity. A flag-shape hysteretic behavior with increased energy dissipation capacity was observed in the experimental studies. Experimental results revealed that small residual displacement upon unloading could be obtained if the ED bar ratio is below a certain threshold. Except for ED bars, researches on the external energy dissipaters also have been conducted. Chou and Chen [6] suggested using concrete-filled tubes as external energy dissipaters, and their results showed that the equivalent viscous damping ratio can be obviously increased. Marriott et al. [7] used two different external replaceable energy dissipaters for unbonded pre-stressed segmental piers and obtained considerable energy dissipation when compared with the traditional hybrid ED bar system. Some previous studies (e.g. [8–10]) showed that monolithic connections between first segment and the footing can result in better energy dissipation than segmental connections under seismic loading. The use of other energy dissipaters were also reported including external steel angles and rubber pads [8] and built-in elastomer pad [9]. Besides using dissipaters, improving the material performance of components, such as using high performance ED bars [10] or ductile fiber-reinforced concrete [11], could lead

* Corresponding author at: Dept. of Bridge Engineering, Southwest Jiaotong University, Chengdu, Sichuan 610031, China.
E-mail address: xzhli@swjtu.edu.cn (X. Li).

http://dx.doi.org/10.1016/j.engstruct.2017.08.018
0141-0296/

to higher drift capacity, greater energy dissipation, and higher lateral strength of the column.

Besides the experimental investigations, a wide range of numerical studies have also been conducted. Solid finite element (FE) model [5,10], fibre-based FE model [12,13] and lumped-mass FE model [5] have been commonly used to capture the local stress of the column or the global response of bridge structure with segmental columns. Detailed 3D solid FE model can capture the local stress or even damage of the column. Its calculation efficiency is however low, which makes it difficult to be applied in the numerical simulation of the whole bridge structure. Fibre-based FE models have been widely used in the seismic response analysis of structures with conventional monolithic piers [14–16]. For the precast segmental columns, complex contact behavior between the segments makes the numerical simulation results with fibre-based model not as good as 3D FE model. Lumped-mass model which assumes the segmental column as a hinge spring with a lumped mass at the top can simulate the global response with computational efficiency. Ou et al. [5] developed a flag-shaped model based on the data from Chang et al. [4] and the 3D FE model. More detailed lumped-mass model which considered the degradation of unloading, reloading and strength [17,18] were developed by using the "Pinching4" material model in OpenSEES [19].

Compared to the extensive experimental and numerical studies on the seismic performances of segmental columns, the investigations on the seismic responses of a whole bridge system with segmental columns are rare and no study that compares the seismic responses of a bridge with segmental columns and with conventional monolithic columns can be found in literature yet. To the best knowledge of the authors, only the following two papers reported the seismic responses of a whole bridge system with precast segmental columns. Sideris et al. [20] carried out a series of shake table tests on a hybrid sliding-rocking (HSR) posttensioned segmental bridge system. The HSR joints were designed to exhibit sliding (slip-dominant, SD) or rocking (rocking-dominant RD) property to mitigate the applied seismic loading and reduce damage. Experimental results showed that the SD joints provided high energy dissipation and moderate self-centering capability. The RD joints, on the other hand, exhibited high self-centering but low energy dissipation capability. Zhang [13] conducted numerical and experimental investigations to evaluate the feasibility of applying steel fiber reinforced self-consolidating concrete to precast unbonded post-tensioned segmental bridge columns in moderate-to-high seismic regions. The test results showed that segmental columns have excellent self-centering capability. Two types of cap beam-superstructure connections, i.e., a connection with non-seismic rubber bearing and a fixed connection, were experimentally tested. Testing results revealed that the fixed connection could induce more impact force at the first joint of the segmental column (counting from the base to the cap beam) comparing with the one with non-seismic rubber bearings.

Many previous experimental and numerical investigations (e.g. [3]) indicated that segmental columns have smaller initial stiffness and smaller energy dissipation capacity than monolithic columns. Moreover, the opening at the joint interfaces may influence the integrity of the columns. These factors may result in large relative displacements between adjacent superstructures of the bridge, which in turn can lead to higher pounding potentials compared to the bridges with conventional monolithic columns. Seismic induced pounding responses between bridges with segmental columns are therefore believed critical and should be considered in the analyses. No literature, however, reports the seismic induced pounding responses between adjacent bridge structures with precast segmental columns though the researches on the conventional bridges are very extensive. For example, Guo et al. [21] carried out shake table tests on a 1:20 scaled two-span base-isolated bridge to investigate pounding behavior of adjacent superstructures. Li et al. [22] experimentally evaluated the influence of spatially varying ground motions on the pounding behavior of three adjacent bridge segments. He et al. [23] conducted large scale (1:6) experimental studies on the pounding responses between two bridge frames. Two boundary conditions, i.e. the fixed foundation and rocking foundation, were tested to investigate the influence of foundation types. Compared to the relatively less experimental studies, the numerical investigations on the pounding responses are extremely rich. Many pounding models (including the stereo-mechanical method, impact element method and 3D arbitrary pounding method) and finite element models (including the lumped mass model, beam-column model, distributed mass model and detailed 3D FE model) have been adopted by different researchers. Hao et al. [24] summarized these methods and models and discussed the pros and cons of these methods. These investigations revealed that pounding can significantly influence the adjacent bridge structural responses, and it may lead to local damages or even collapse to the bridge structures. Many methods have also been proposed to mitigate these adverse effects. Shrestha et al. [25] provides an intensive review on the devices to protect bridge superstructures from pounding and unseating damages. It should be noted that all the studies were focused on the bridge structures with conventional monolithic bridge columns, no literature reports pounding responses between adjacent bridge structures with segmental columns yet.

This paper carries out numerical simulations on the seismic responses of bridge structures with precast segmental columns by using the finite element code OpenSEES. For comparison, the seismic responses of the bridge with conventional monolithic columns are also calculated. Seismic induced pounding responses are considered in the numerical simulations. The hysteretic behaviors of the segmental column and monolithic column are firstly modelled and validated by the experimental results. The validated column models are then applied to the whole bridge systems to calculate the structural responses. The influences of pounding, frequency ratio and gap size are investigated and discussed. It should be noted that ground motion spatial variations and soil-structure interaction (SSI) can further influence the structural responses. Not to further complicate the problem, they are not considered in the numerical simulations.

2. Bridge model

Without loss of generality, a typical five-span continuous bridge extensively investigated by other researchers (e.g. [13,20,26]) is adopted in the present study as the reference bridge model with minor modifications on the span length and pier height. Fig. 1 shows the elevation view of the bridge and Fig. 2(a) shows the cross section of the box-girder. As shown, this bridge is a single cell box-girder bridge with a width of 8.4 m and height of 1.8 m. The length of the side span is 20 m and the lengths of the three middle spans are 30 m. The height of the four piers is 10 m. One expansion joint is located at the middle of the bridge and another two locate at the abutments. The size of the expansion joints is 0.1 m. For easy reference, the parameters of the girder and columns are presented in Table 1.

To investigate the influence of different column types, segmental column and monolithic column are considered in the present study. Wang et al. [27] carried out large-scale experimental studies to investigate the hysteretic behavior of segmental columns, the specimen experimentally investigated in [27] is directly used in the present study and Fig. 2(b) shows the details of the segmental column. As shown, the column includes 9 segments (S1 to S9). The height of the bottom segment is 2 m and the height of the rest 8

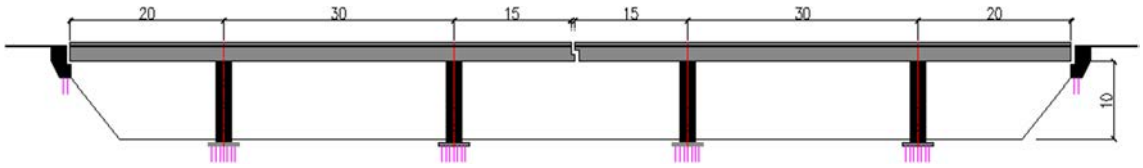

Fig. 1. Elevation of the bridge model (m).

segments is 1 m. The cross section of the column is also shown in the figure. As shown, six 7T D15 (15 mm in diameter) pre-stressed tendons are installed to provide the pre-stressed force and self-centering capability of the column. D22 longitudinal mild steel bars are used in each segment to position the transverse reinforcements (the stirrups, which are not shown in the cross section). D36

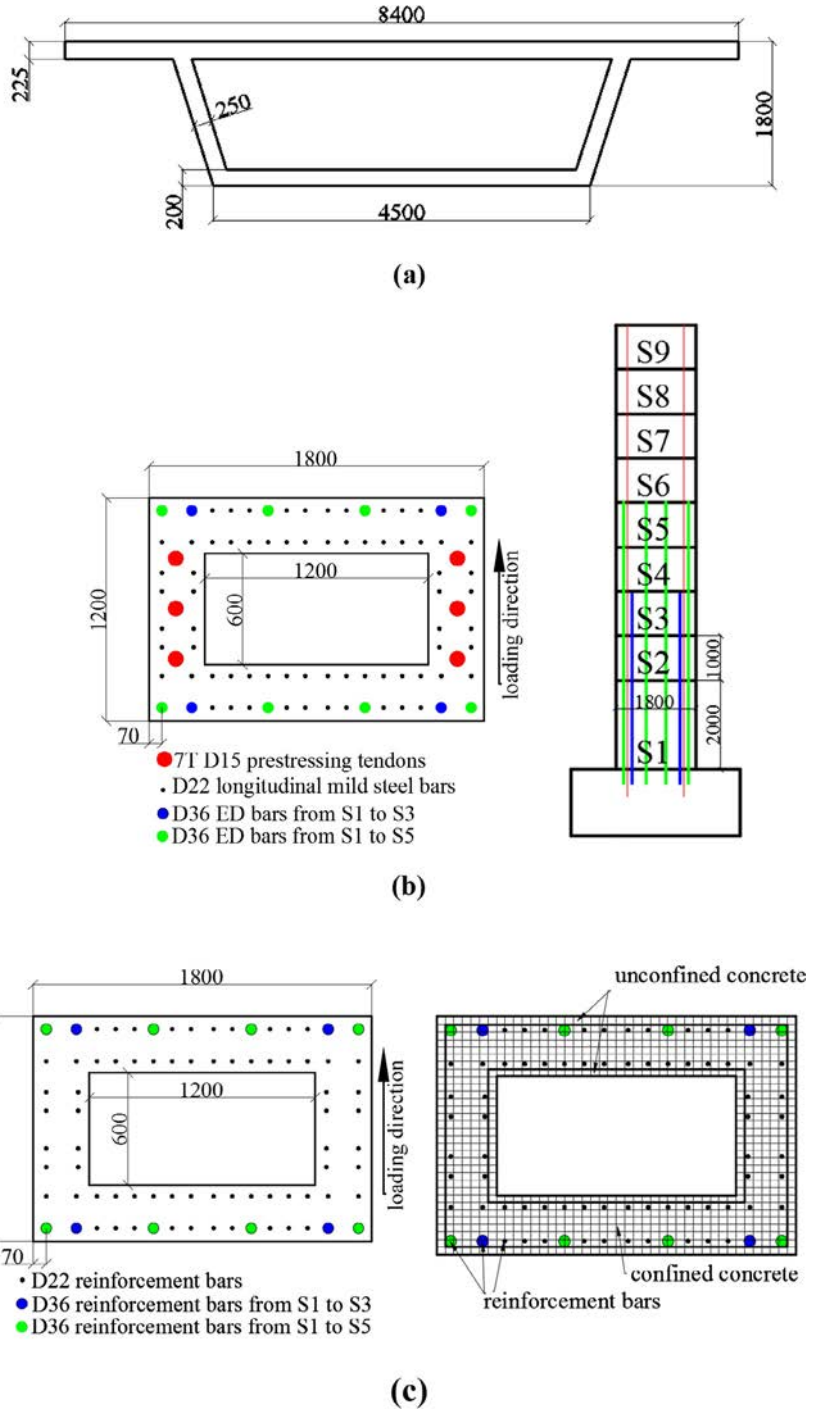

Fig. 2. Details of the bridges, (a) cross-section of box-girder; (b) Details of the precast segmental column (after [27]) and (c) details and fiber discretization of the monolithic column section (mm).

Table 1
Cross-sectional properties and reinforcing steel ratios of structural components.

Structural component	Cross sectional area, A (m^2)	Moment of inertia, I (m^4)	Tendon ratio, ρ1 (%)	ED bar ratio, ρ2 (%)	Longitudinal steel bar ratio, ρ3 (%)
Girders	3	1.74	/	/	/
Segmental columns	1.44	0.24	0.41	S1-S3:0.85 S3-S5:0.57	1.6 (in segment only)
Monolithic columns	1.44	0.24	/	S1-S3:0.85 S3-S5:0.57	1.6 (continuous)

longitudinal mild bars are used as ED bars. Eight D36 bars (the green dots in the figure) extend continuously from S1 to S5 and another four (the blue dots) are only within the bottom three segments (S1 to S3).

Fig. 2(c) shows the cross section of the monolithic column. For a fair comparison, the longitudinal reinforcement ratio in the segmental column and monolithic column are designed almost the same. Particularly, the same number of longitudinal mild steel bars is used in the monolithic column but they are extended along the whole height of the column. No pre-stressed tendons are designed in the monolithic column. Cyclic loading is applied in the weak axis of the two columns.

3. Numerical model and validation

3.1. Segmental column

As mentioned above, the segmental column experimentally investigated by Wang et al. [27] is directly used in the present study. The detailed information regarding the segmental column has been presented in Section 2.

To simulate the hysteretic behavior of segmental column under cyclic loading, the lumped-mass model shown in Fig. 3(a) is adopted. As shown, the mass of the segmental column is lumped at the top of the column, and it is connected to a 2 D rigid beam element, which has the same height as the column. The bottom of the rigid beam is connected to a zero-length element with "Pinching4" material in OpenSEES to capture the global hysteretic behavior of the column. Previous studies (e.g. [17,18]) revealed that this simplified lumped-mass model can capture the global response of the column with computational efficiency. To examine the accuracy of the simplified model, the loading protocol (Fig. 3 (b)) that was used in the experimental study [27] is applied to the simplified model.

Fig. 4(a) shows the constitutive curve of the "Pinching4" material. As shown, this model is composed by piecewise linear curves and represents a "pinched" load-deformation response. The cyclic degradation of strength and stiffness can also be considered by this model. This model, which was originally developed to simulate the seismic response of beam-column joints, was also used to capture the characteristics of other structures, such as the cross-laminated-timber shear walls [28], the masonry infill walls [29], and the dis-

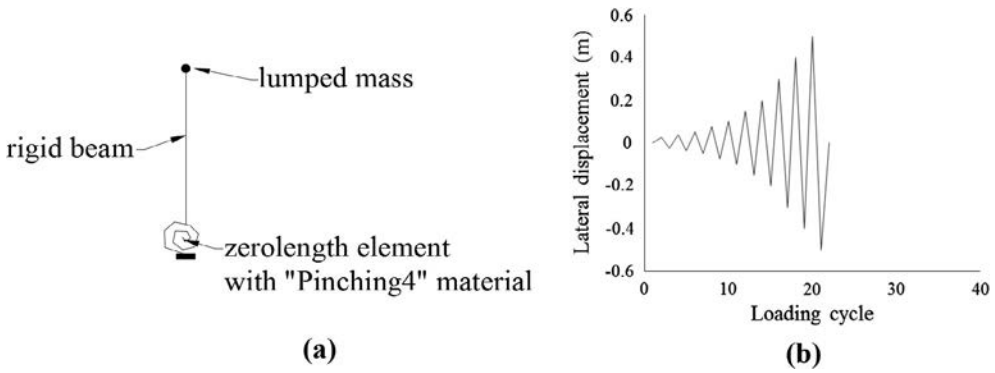

Fig. 3. Numerical modelling of segmental column, (a) lumped-mass model with Pinching 4 material; (b) Cyclic loading protocol.

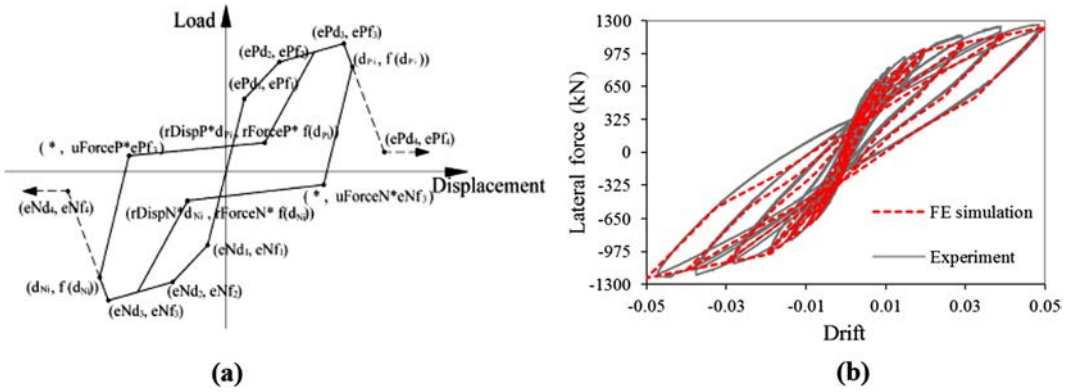

Fig. 4. Numerical modelling of segmental column, (a) load–displacement relationship of "Pinching4" model; (b) Comparison of the calculated hysteretic curve with the testing results.

Table 2
Parameters for the "Pinching4" model used in the numerical simulation.

Parameters	Value
ef1 ~ 4, defining force envelope (MN·m)	±8* ±12 ± 12.8 ± 13
ed1 ~ 4, defining deformation envelope (10–2 rad)	±0.89 ± 3.9 ± 5 ±5.2
rDispP/rDispN, ratio of deformation during reloading	0.5
rForceP/ rForceP, ratio of force during reloading	0.6
uForceP/ uForceN, ratio of strength during unloading	−0.4
gK1 gK2 gK3 gK4 gKLim, unloading stiffness degradation	1.0 0.0 1.0 0.0 1.0

* $ePf_1 = +8$, $eNf_1 = -8$.

sipative connections for brace to column joints [30], etc. As shown in Fig. 4(a), in total 22 parameters need be defined in order to capture the hysteretic behavior of the segmental column. All these parameters are defined based on the experimental results. Table 2 tabulates the corresponding values used in the present study. The meaning of each parameter is not presented in this paper. Interested readers can refer to the OpenSEES User's manual [19] to find more detailed information. Fig. 4(b) shows the comparison between the experimental data and the numerical result. It can be seen that this model can capture the hysteretic behavior of segmental column accurately.

It should be noted that in using this lumped-mass model to represent the true performance of the structure under seismic motions, proper parameters need be defined. An experimental study is normally required to accurately determine these parameters. To develop a high efficiency numerical model without the aid of testing data is a very interesting topic but is out of the scope of the present study.

3.2. Monolithic column

Wang et al. [27] only tested segmental columns in their study. Another test carried out by Tanaka and Park [31] is used to calibrate the numerical model of monolithic column.

Specimen tested in [31] was a 1.65 m cantilever column with a square cross section. The sectional details and material parameters are shown in Fig. 5 and Table 3 respectively. To simulate the hysteretic behavior of the monolithic column, a fiber-based beam-column element model is developed in this study. Uniaxial material concrete06, which is based on the constitutive model developed by Mander & Priestley [32], is used to model the unconfined and confined concrete fibers. The modified reloading path of the model could capture the bond-slip behavior and residual displacement of fiber-based element model under seismic loading [14]. The uniaxial material Giuffre-Menegotto-Pinto steel02 [33] is used to simulate the steel rebars.

Fig. 6 shows the comparison of the simulated and tested hysteretic behavior of monolithic column. As shown the numerical model can reasonably capture the hysteretic behavior of the monolithic column, which demonstrates the accuracy of the numerical model.

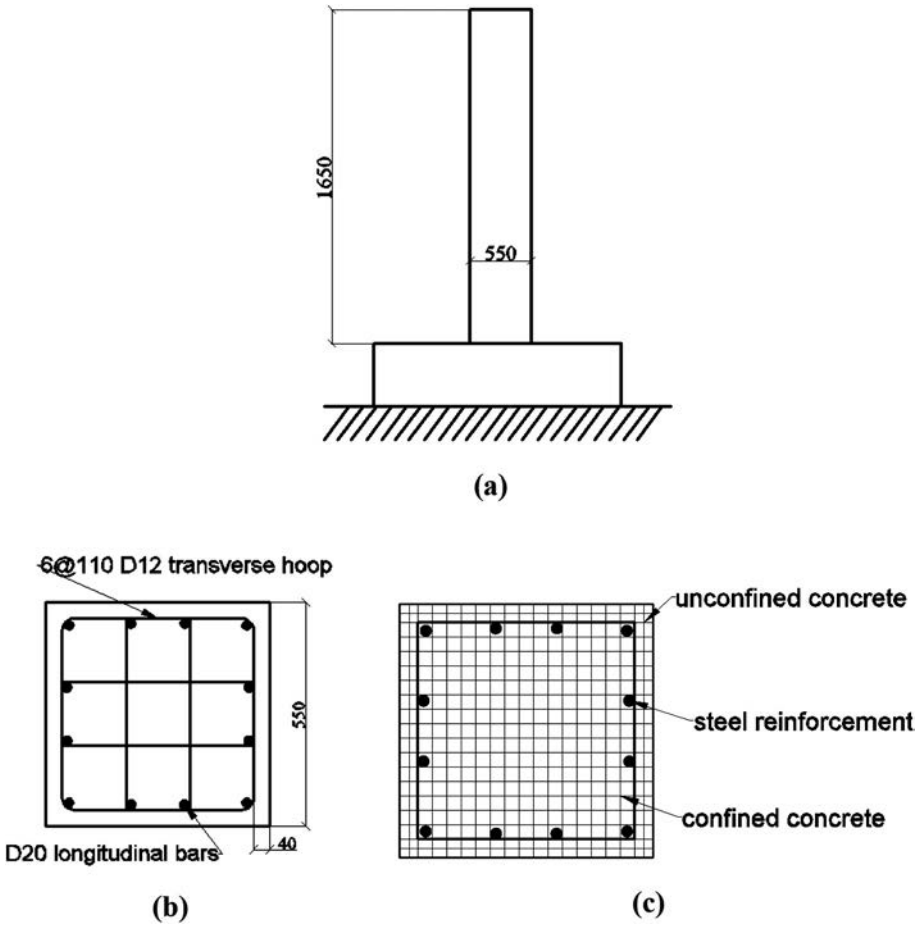

Fig. 5. Details of cantilever column (after [31]). (a) General information; (b) Cross section; (c) Fiber discretization of the section (mm).

Table 3
Material parameters of monolithic cantilever column (after [31]).

Concrete strength (MPa)	Axial load (kN)	Longitudinal reinforcement ratio (%)	Yield strength of longitudinal steel bars (MPa)	Transverse reinforcement ratio (%)	Yield strength of transverse steel hoops (MPa)
32	968	1.25	511	1.7	325

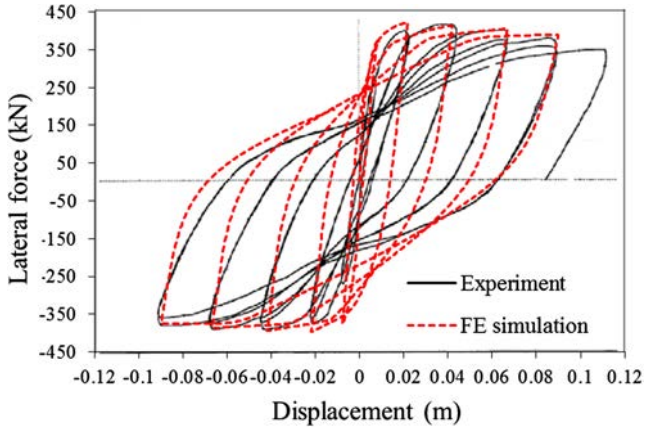

Fig. 6. Hysteretic curve calibration of monolithic column using fibre-based model.

3.3. Comparisons of hysteretic behaviors of monolithic and segmental columns

The validated model is used to calculate the hysteretic behavior of the monolithic column shown in Fig. 2(c). Fig. 7 shows the calculated hysteretic curve of the monolithic column. For comparison, the hysteretic behavior of the segmental column obtained in Section 3.1 is also plotted in the figure. Table 4 compares the important parameters of these two columns.

In the experimental study of segmental column [27], the specimen was tested up to a drift ratio of 5%. In the numerical simulations, the drift ratios of both the segmental and monolithic columns are also calculated up to 5%. It can be seen that with a 5% drift ratio, the residual displacement of segmental column (0.085 m) is much smaller than that of monolithic column (0.306 m), which demonstrates good self-centering capability of segmental column. The hysteretic curve shows that the stiffness of the monolithic column begins to decrease after a drift ratio of about 2%. For the segmental column, no obvious stiffness degradation is observed. The maximum lateral loading for the monolithic and segmental columns are 1320 and 1280 kN respectively. The

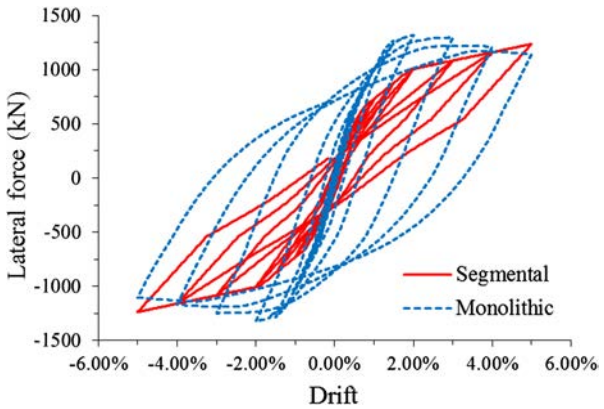

Fig. 7. Comparisons of the hysteretic behaviors of monolithic and segmental columns.

Table 4
Property comparisons of monolithic and segmental columns.

Column type	Residual displacement at 5% drift (m)	Maximum lateral loading (kN)	Equivalent viscous damping ratio (%)
Monolithic	0.306	1320	30.16
Segmental	0.085	1280	9.51

lateral loading at 5% drift ratio of the segmental column is slightly larger than that of monolithic column, indicating more severe strength degradation of the monolithic column due to concrete damage and reinforcement yielding.

To examine the energy dissipation capacity of the segmental column and monolithic column, the commonly used equivalent viscous damping ratio, which is defined as $\xi_{eq} = A_h/2\pi A_e$ [34], is adopted in the present study. In this formula, A_h represents the area enclosed by one complete idealized load–displacement hysteresis loop and A_e is the elastic strain energy in an equivalent linear elastic system under static conditions. With this definition, the equivalent damping ratios for the monolithic and segmental columns with a 5% drift ratio are 30.16% and 9.51% respectively based on the hysteretic curves shown in Fig. 7. It is obvious that much less energy is dissipated by the segmental column compared to the monolithic column.

4. Numerical modelling of bridge structures with different columns

The FE code OpenSEES is used to develop the FE models of the bridge structures with two types of columns. Fig. 8(a) and (b) show the FE models of the bridges with segmental and monolithic columns, respectively. The bridge girder is modelled by the 2 D elastic beam-column elements, and no plastic deformation is considered in this study [24]. The Young's modulus is assumed as E_c = 32.5 GPa and other properties can be found in Table 1. The segmental columns are simulated by the lumped-mass model with "Pinching4" material as discussed in Section 3.1 and the monolithic columns are modelled by the fiber-based model as described in Section 3.2.

The abutments are modelled by two separate nonlinear springs representing the pile stiffness and passive soil stiffness as shown in Fig. 8. As indicated in [35], the initial stiffness of the piles degrades with the yielding of soil, so the bilinear symmetrical model which acts in both active and passive loadings of the abutments is used to model this effect. 24 piles are placed in each abutment and they are assumed to become plastic at a deformation of 25 mm. The ultimate strength of 4 MN is adopted based on a similar bridge as reported in [16]. Fig. 9(a) presents the load-deformation curve for the abutment piles. Zero-length element with elastic-perfectly plastic material in OpenSEES is adopted to model the piles. As for the passive soil embankment, elastic plastic spring with initial stiffness of 200 MN/m and ultimate strength of 10 MN is adopted [16]. Fig. 9(b) shows the load-deformation curve for soil embankment and zero-length element with elastic-perfectly plastic gap material in OpeenSEES is used to simulate the passive action of soil embankment. The initial gap size between the back fill soil and the abutment is assumed to be 0 mm in the numerical model. The unloading stiffness of both piles and

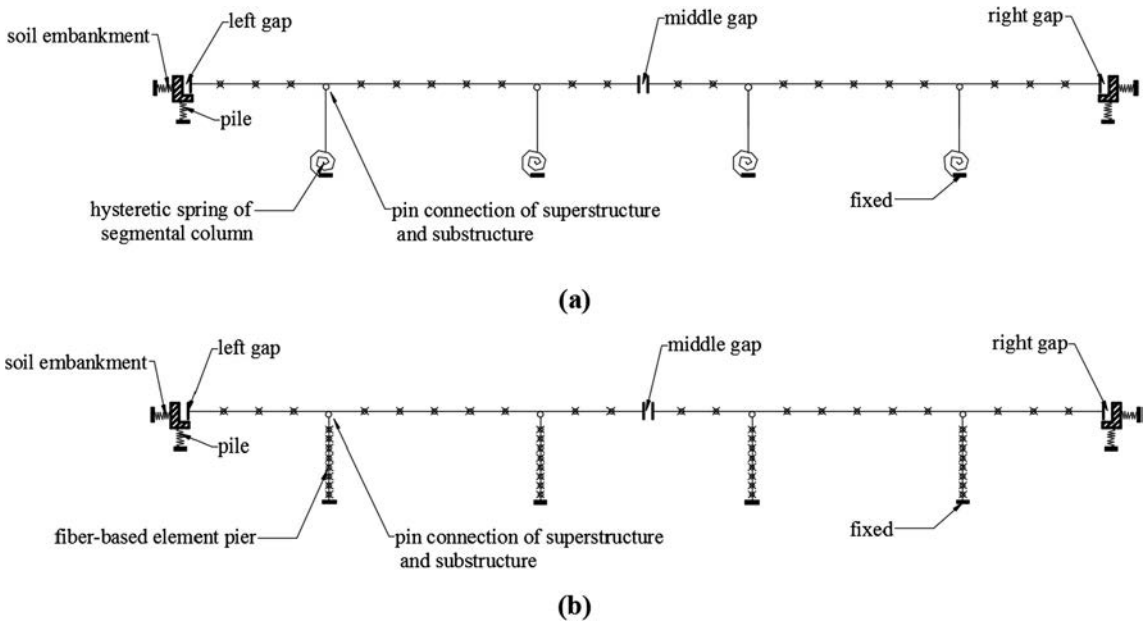

Fig. 8. Finite element models of the bridge structures, (a) bridge with segmental columns and (b) bridge with monolithic columns.

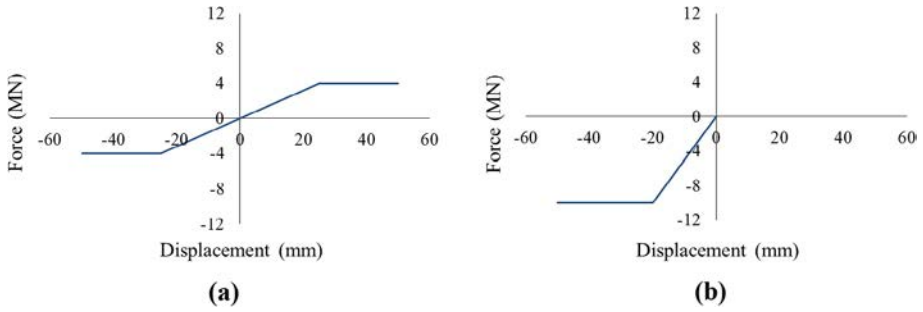

Fig. 9. (a) Force-displacement model of abutment piles and (b) force-displacement model of soil embankment.

embankment were assumed as the same with the loading stiffness and permanent deformation will be formed if they entered plastic stage.

It should be noted that the simplifications shown in Fig. 9 neglect the influence of damping, which might result in slightly larger structural responses. However, the primary aim of this study is to investigate the influence of different column types on the seismic responses of bridge structures, this simplification is believed not influence the conclusion of the paper. This simplification is actually adopted by many researchers (e.g. Shrestha et al. [16]) for its simplicity.

With the FE models, the vibration periods and vibration modes of the bridge system with different columns can be calculated by carrying out an eigenvalue analysis. It is found that the fundamental periods of one bridge frame (either the left or right frame in Fig. 8) are 1.075 s and 1.323 s when the bridge is supported by the monolithic column and segmental column respectively. The bridge supported by segmental column is slightly flexible than that supported by the monolithic column. This is expected because the formation of the segmental column with a pile of segments introduces more flexibilities to the column as compared to the monolithic column. The fundamental vibration modes are the same for the two bridge structures, and it is dominated by the longitudinal movement of the bridge girder.

4.1. Impact element modelling

Seismic induced poundings might occur at the expansion joints during a severe earthquake, which could significantly affect the seismic responses of bridge structures. Therefore possible pounding between adjacent bridge super structures at the expansion joint and between bridge girder and abutment are considered in the present study. Many different methods have been developed to simulate the pounding phenomenon between adjacent structures and the most common way is using the contact element model. In a contact element, the stiffness of the impact element (K_I) should be defined. In the present study, the pounding along the longitudinal direction of the bridge is considered and the stiffness is calculated as [15,16]

$$K_I = \gamma E_c A / L \tag{1}$$

where E_cA is the stiffness of the axial cross section of the superstructure, L is the length of the bridge girder and γ is the ratio of impact spring stiffness to the stiffness of the superstructure, which is taken as 2 according to a sensitivity analysis [15] with similar superstructures. K_I is therefore calculated as 6.5 GN/m in the present study. It should be noted that during pounding, some energy can be dissipated. Not to further complicate the problem this is however neglected in the present study. This is actually a common

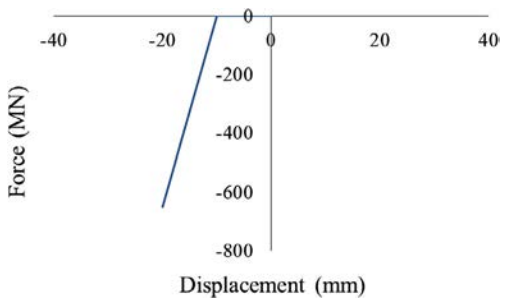

Fig. 10. Impact element.

practice in the numerical modelling, many previous studies (e.g. [15,16]) neglected energy dissipation during pounding in the numerical model. It also should be noted that many previous studies (e.g. [36]) revealed that the structural responses are not sensitive to the selected pounding stiffness of the impact element, the selection of γ in Eq. (1) will therefore not obviously influence the numerical results.

Zero-length element with elastic-perfectly plastic gap material (shown in Fig. 10) in OpenSEES is adopted to simulate the pounding phenomenon between bridge girders and between bridge girder and the corresponding abutment. Without loss of generality, a gap size of 0.1 m is assumed in the present study. Parametric studies are also carried out to investigate the influence of gap size on the structural responses.

4.2. Damping

Damping can influence the structural response in the nonlinear time history analysis of structures. The Rayleigh damping model, which is widely used in the distributed plasticity model, is shown to develop 'spurious' damping forces and lead to inaccurate response results, especially for the concentrated plasticity model.

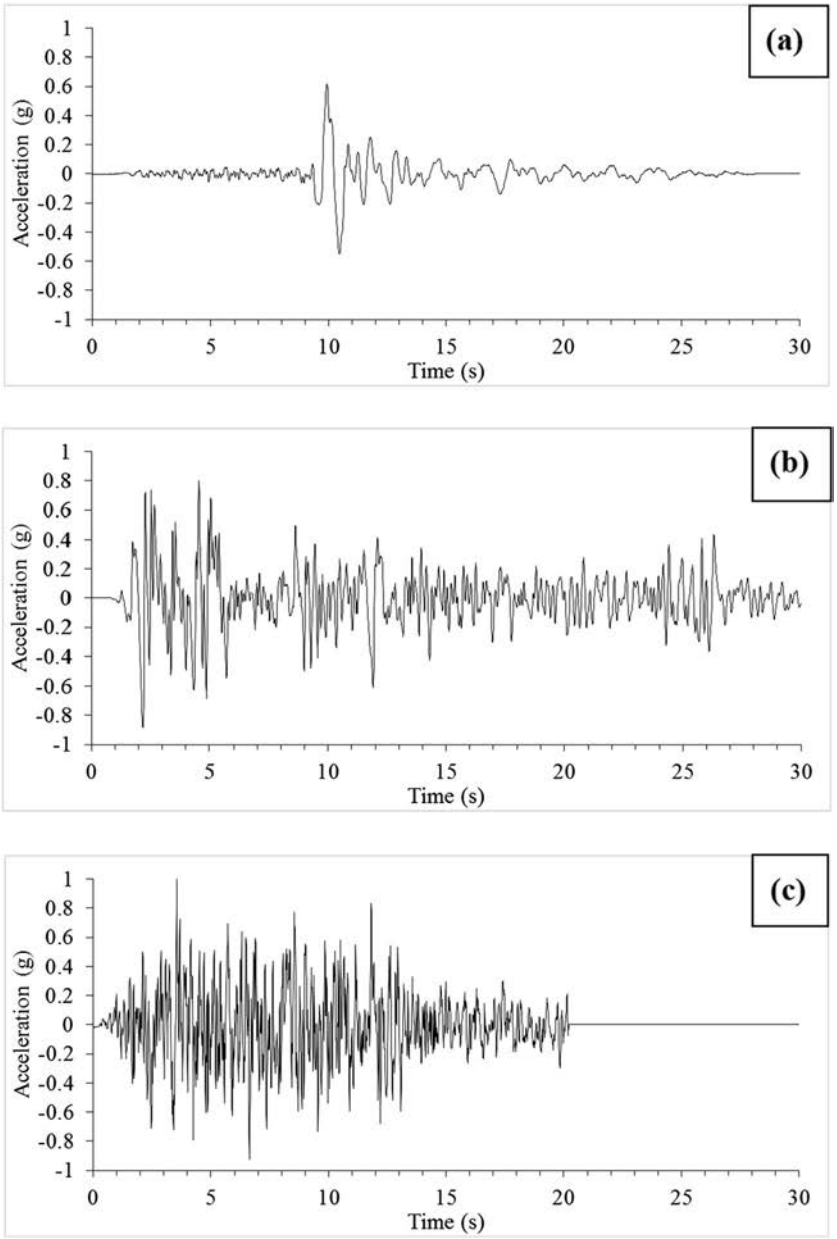

Fig. 11. Different acceleration time histories. (a) SMART1 earthquake, (b) El-Centro earthquake and (c) artificially simulated earthquake.

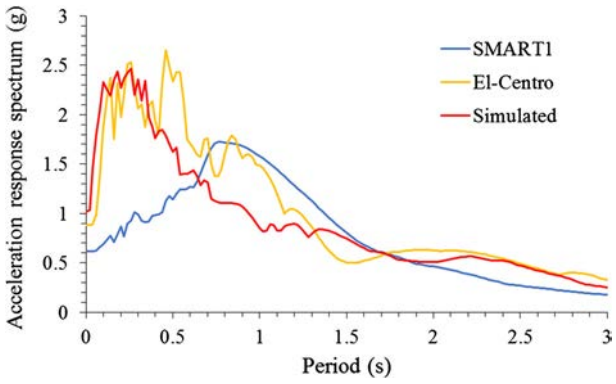

Fig. 12. Acceleration response spectra of the three earthquake ground motions.

Chopra and McKenna [37] proved that a viscous damping matrix constructed by superposition of modal damping matrices-irrespective of the number of modes included or values assigned to modal damping-completely eliminates the 'spurious' damping forces. OpenSEES has recently been extended to be able to consider modal damping in the analysis [37]. The more accurate modal damping is applied in the present study to calculate the structural responses. The damping ratio for each vibration mode is assumed as 5%.

4.3. Earthquake loading

Three different earthquake loadings are used as inputs to calculate the structural responses in the numerical simulation. The first earthquake loading is the record from the SMART1 array (event 40, 1986) located in Lotung Taiwan, and the data is downloaded from the Pacific Earthquake Engineering Research Center (PEER [38]). This earthquake loading is characterized by the long-period pulse-like waveforms, and it is normally classified as near-fault ground motion. It should be noted that the peak ground acceleration (PGA) of the original data is 0.2 g, to more clearly see the influence of monolithic and segmental columns, the PGA is scaled to 0.6 g in the numerical simulation. The second record is from the 1940 El-Centro earthquake, which exhibits fewer long-period characteristics and it is used to represent a far-field earthquake. The PGA of this earthquake loading is scaled to 0.8 g. The third earthquake loading is an artificially simulated ground motion. The ground motion time history is simulated to be compatible with the design spectra specified in the New Zealand Earthquake Loading Code [39] by using the spectral representation method proposed by Li et al. [40]. The PGA is set as 1.0 g in the numerical simulation. Fig. 11 shows the acceleration time histories used in the analyses in this study. The corresponding acceleration response spectra are shown in Fig. 12.

5. Numerical results

5.1. Seismic response of one bridge frame

This section investigates the seismic responses of one bridge frame (for example, the left frame in Fig. 1) with different column types under different earthquake loadings. The influence of pounding is not considered in this section, i.e. the size of the expansion joints at the abutment and at the middle of the bridge is assumed large enough and the bridge frame can vibrate freely during the earthquakes. It should be noted the duration for the earthquake loadings shown in Fig. 11 is 30, 30 and 20.48 s respectively. To capture the residual displacement, the simulations are carried out until the bridge structure becomes still. As shown in Fig. 13, the bridge structure almost stops vibrating when the time reaches 40 s under these three earthquake loadings.

Fig. 13 shows the longitudinal deck displacements of the bridge frame with monolithic and segmental columns. As expected, when segmental columns are used to support the bridge deck, much smaller residual displacements are obtained as compared with the one supported by the monolithic columns. As shown, the residual displacements are 0.100, 0.095 and 0.156 m respectively for the bridge with monolithic columns. When segmental columns are used, the corresponding values reduce to 0.044, 0.040 and 0.030 m, with the reduction ratio reaching 56.0%, 57.9% and 80.7% respectively. This is because the pre-stressing tendons as shown in Fig. 2 can provide good self-centering capability to the columns, which in turn results in the smaller residual displacements as demonstrated in the hysteretic curves of the bridge columns (Fig. 7). The results also show that larger peak ground acceleration (PGA) does not necessarily result in the larger residual displacement, this is because the structural response is not only related to the amplitude but also influenced by the frequency contents of the earthquake loading. The results also indicate that when the bridge structures are subjected to the SMART1 earthquake and El-Centro earthquake the reduction ratios are more or less the same (56.0% and 57.9%). When the bridges are subjected to the simulated earthquake, a much larger reduction ratio is obtained (80.7%). This is because as shown in Fig. 13(c), the bridge supported by the monolithic columns experiences large plastic deformation after around 8.8 s, which results in the large permanent deformations of the structure. These results demonstrate the advantages of using segmental columns when large earthquake shakings are expected because segmental columns have very good deformation recovery capability.

Fig. 13 also shows that bridge structure supported by the segmental columns generally results in larger structural responses compared to that supported by the monolithic columns. As shown in Fig. 13, the fluctuations of the red curve are more severe than the blue curve, and it takes more number of cycles for the red curve to come to rest. This can be explained by the equivalent damping ratio shown in Table 4 and the force–displacement relationships shown in Fig. 14. As shown the areas enclosed by the red curve (segmental column) are much smaller than those enclosed by the blue curves (monolithic column), which means less seismic energy is dissipated by the segmental columns and more energy is transferred to the superstructure, this in turn leads to the more severe super-structural vibrations. This may be regarded as a disadvantage of segmental bridge. The peak displacement of the bridge with segmental columns, however, is not necessarily always larger than that with monolithic columns. As shown in Fig. 13, when the bridge structures are subjected to the SMART1 and El-Centro earthquakes, the peak displacements developed in the bridge with segmental columns are slightly larger than those in the bridge with monolithic columns. When the two bridges subjected to the simulated earthquake ground motion, the opposite results are, however, observed. A detailed examination of the response time histories reveal that the large residual responses of monolithic column as shown in Fig. 7 and the ground motion phase contribute to the larger plastic responses of monolithic column than the segmental column. When the monolithic column yields and endures some plastic deformation, the residual deformation is significantly larger than that of the segmental column. Therefore the monolithic column vibrates at a new baseline with a larger plastic deformation when ground motion changes the direction as shown in Fig. 13 (c). As a result, the peak response of the monolithic column supported bridge is even slightly larger than that of the flexible segmental column supported bridge.

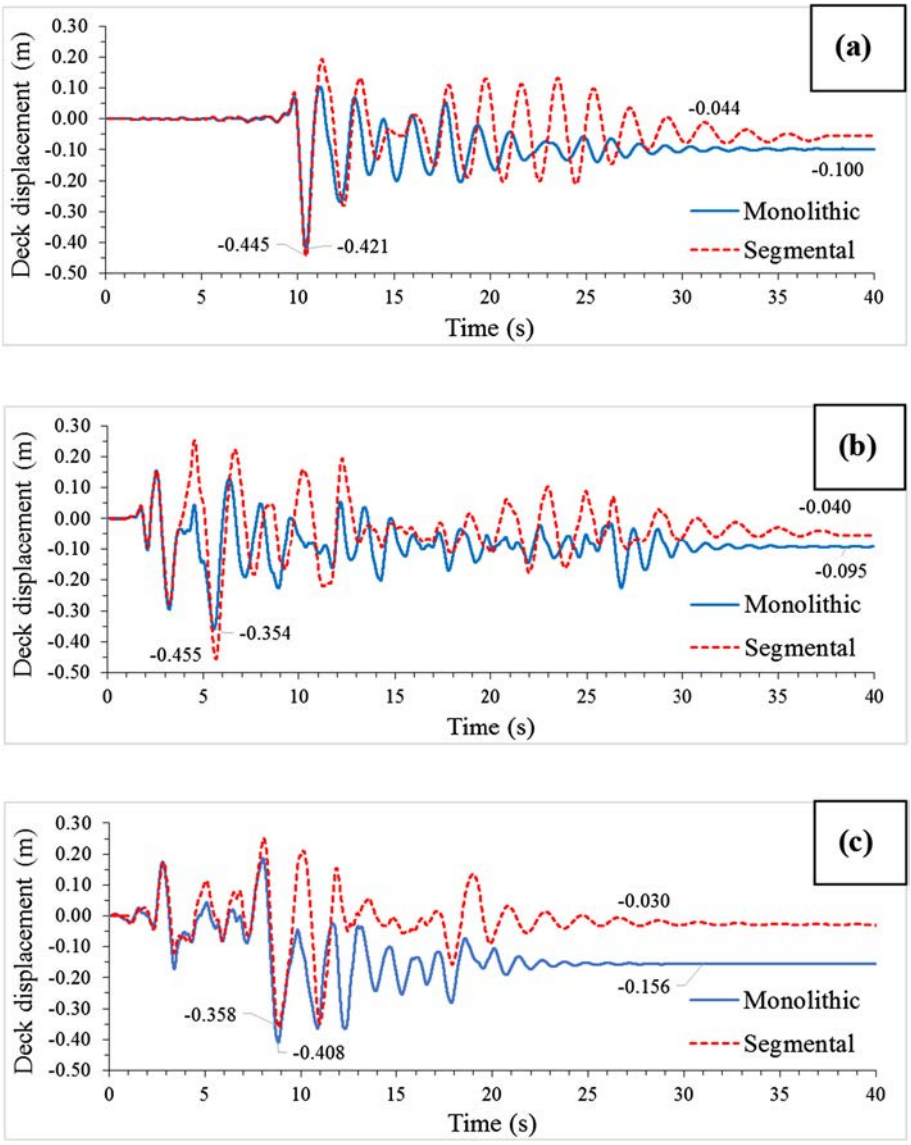

Fig. 13. Deck displacement time histories of one bridge frame under different earthquake loadings. (a) SMART1 earthquake, (b) El-Centro earthquake and (c) artificially simulated earthquake.

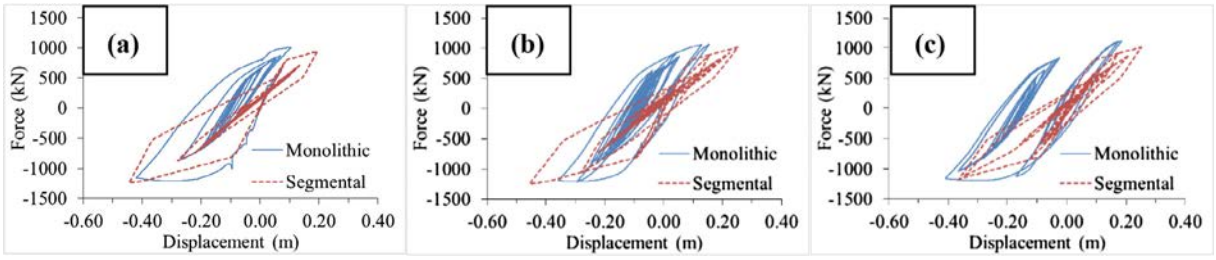

Fig. 14. Force-displacement relationships of bridge structures without the influence of pounding, (a) SMART1 earthquake, (b) El-Centro earthquake and (c) artificially simulated earthquake.

5.2. Influence of pounding

In the previous section, only one bridge frame is investigated and the influence of pounding is not considered. The seismic responses of the whole bridge structure are investigated in this section and the influence of pounding is considered. As shown in Fig. 1, the two frames of the bridge is symmetric, the vibration characteristics of the two frames are therefore the same. Adjacent structures with identical dynamic characteristics under uniform earthquake loading will vibrate in phase and no pounding will occur if there is no restraint from the abutments. Because of the restraints provided by the abutments, poundings can occur and further influence the structural responses. Due to the symmetry of the structure, only the results of the left bridge frame are pre-

sented and discussed. The seismic responses of the bridge with different column types, including the deck displacement, pounding force and pounding times, are compared and discussed. The gap size at three locations is the same in this section, and it is assumed as 0.1 m.

Fig. 15 shows the longitudinal deck displacement of the bridge frame supported by different columns with the effect of pounding. As shown, when pounding is considered, the residual displacements of the both bridges reduce obviously compared to the case without pounding as shown in Fig. 12. For the bridge with monolithic columns, the reduction ratios are 24.0%, 47.4% and 84.0% respectively with an average of 51.9% for the three earthquake ground motions. For the bridge with segmental columns the reduction ratios are 40.9%, 20.0% and 40% with an average of 33.4%. Therefore pounding might be regarded as beneficial in terms of reducing the bridge residual displacement especially for the monolithic bridge. However, it should be noted that this does not mean very small separation gap or even no gap should be designed in engineering practice. Separation gap has many functions, for example it is necessary for the expansion and contraction of the superstructure due to changes in temperature.

Compared to those in Fig. 14, Fig. 15 also shows that the restraints from the adjacent bridge frame and abutment obviously reduce the peak displacements of both bridge structures. For the bridge with monolithic columns, the reduction ratios are 15.8%, 20.9% and 51.5% respectively with an average of 29.2% and for the bridge with segmental columns, the reduction ratios are 23.1%, 35.8% and 37.2% for the three different earthquake loadings with the average of 32.0%. Similar to the case without considering pounding, the bridge structure with segmental columns experiences more severe super-structural vibrations (Fig. 15) due to the fact that less energy is dissipated by the segmental columns as shown in Fig. 16.

Fig. 17 shows the impact force time histories at the left and middle expansion joints under different earthquake loadings. As can be seen, for both bridges, the pounding forces obtained at the left expansion joint are generally smaller than those at the middle expansion joints. This is because the mass of the abutment is 40,000 kg and the mass of the bridge deck is 453,300 kg. At the left expansion joint, poundings occur between the abutment and bridge girder while at the middle expansion joint, poundings occur between two bridge girders. Less mass is involved in the poundings

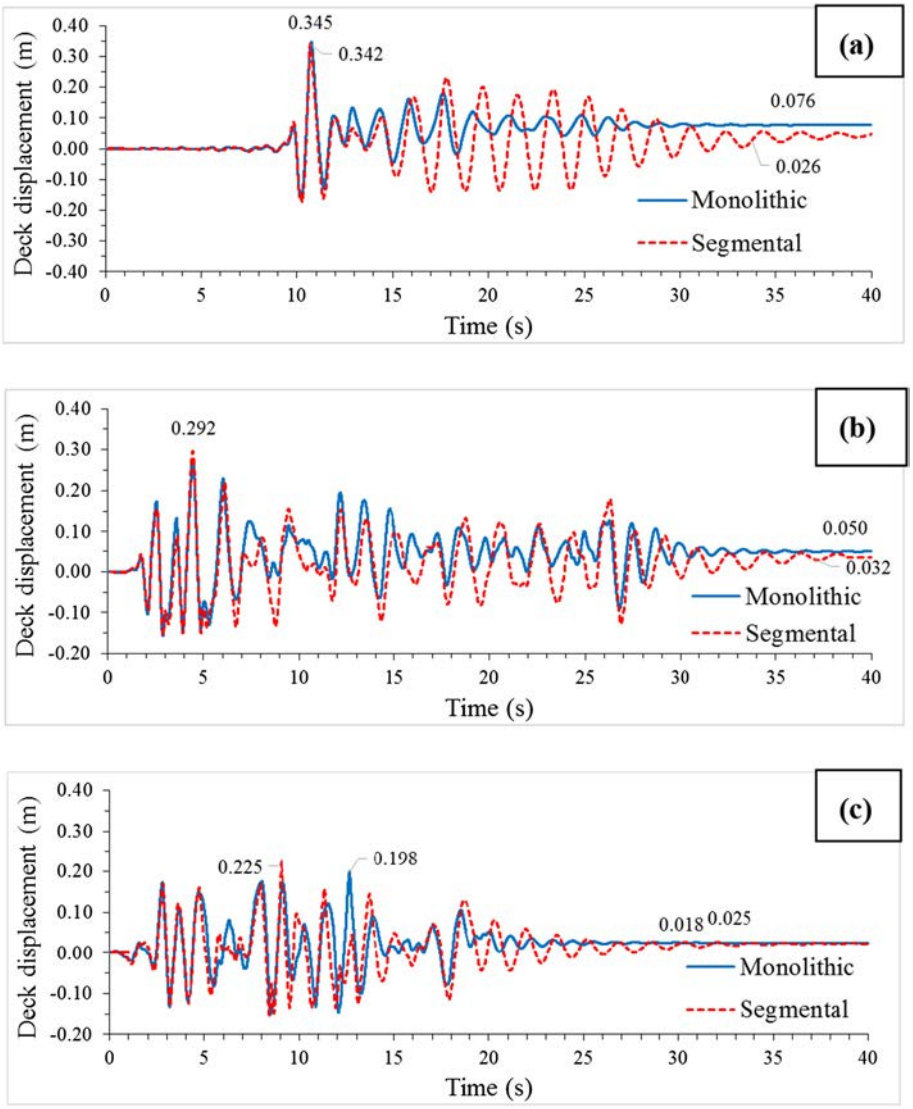

Fig. 15. Deck displacement time histories of left bridge frame under different earthquake loadings with the influence of pounding. (a) SMART1 earthquake, (b) El-Centro earthquake and (c) artificially simulated earthquake.

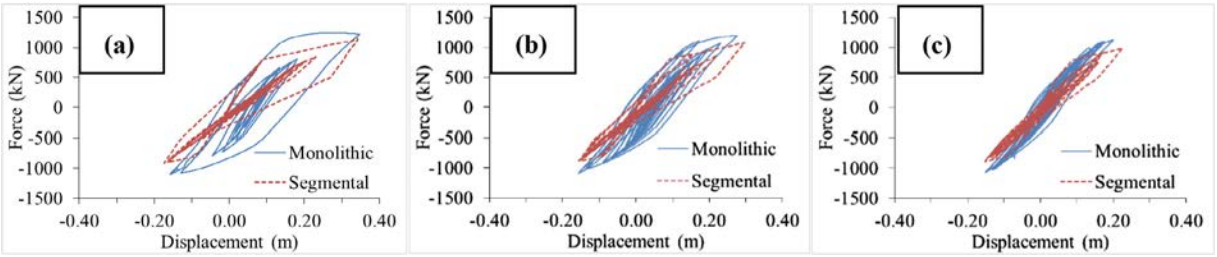

Fig. 16. Force-displacement relationships of different bridge structures with the influence of pounding. (a) SMART1 earthquake, (b) El-Centro earthquake and (c) artificially simulated earthquake.

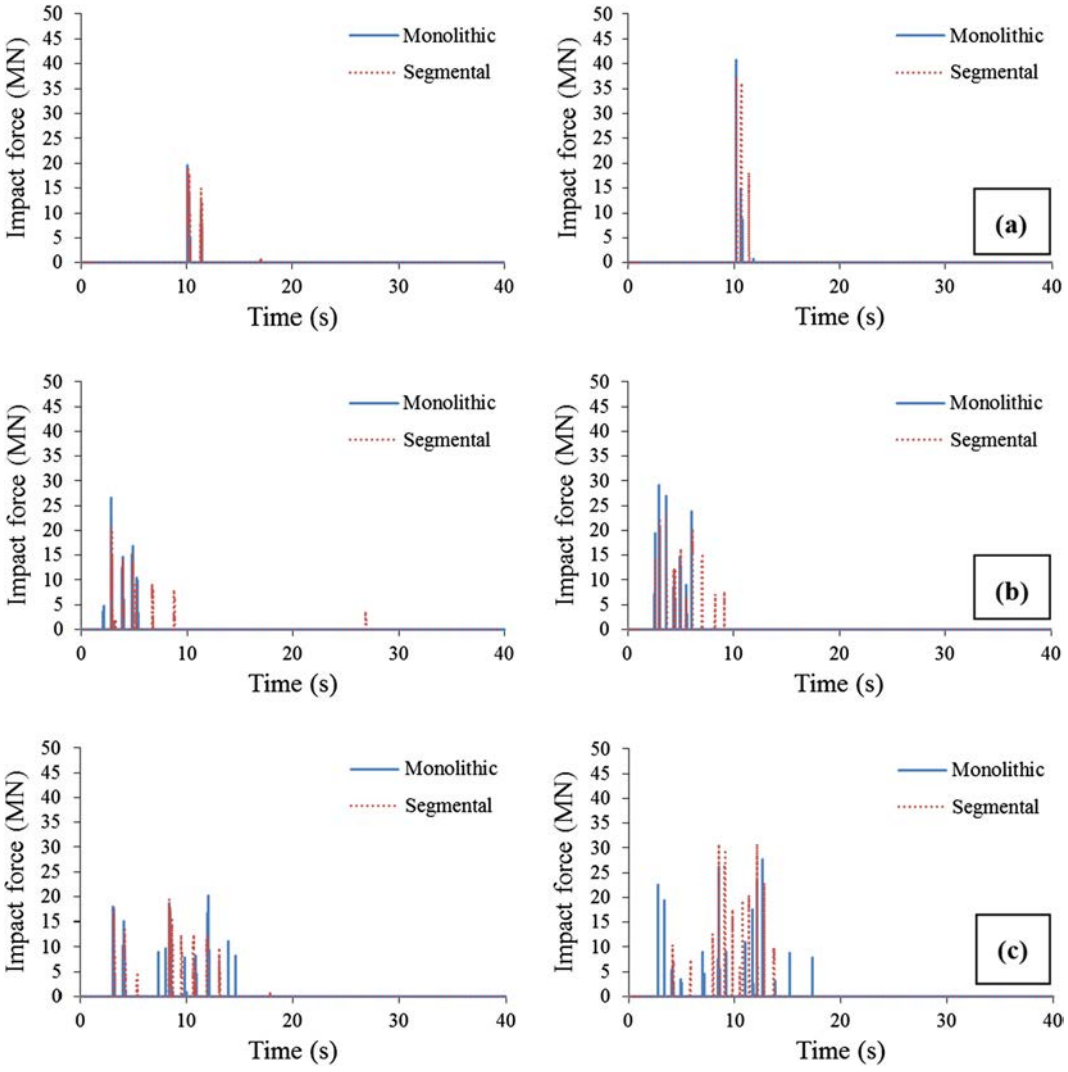

Fig. 17. Impact force time histories at the left and middle expansion joints under three earthquake loadings. (a) SMART1 earthquake, (b) El-Centro earthquake and (c) artificially simulated earthquake.

occurring at the left expansion joint compared to those occurring at the middle expansion joint. Smaller mass leads to smaller inertial resistance and smaller pounding force.

Table 5 tabulates the number of poundings under different earthquake loadings. As can be seen from the table, the number of pounding occurring at the middle expansion joint is generally more than (or equal to) that at the left expansion joint for both bridges. This is because pounding at the middle gap occurs when the relative displacement between the two bridge decks is larger than the separation gap, while at the left expansion joint, it is determined by the relative displacement between the bridge deck and left abutment. The bridge abutments vibrate relatively slow under seismic loadings and therefore generate less number of poundings. Table 5 also shows that when the bridges are subjected to the SMART1 earthquake and El-Centro earthquake, the bridge with segmental columns results in more number of poundings compared to the bridge with monolithic columns. This is because both bridge columns exhibit certain extent of inelastic deformation and less energy is dissipated by the segmental columns (see Fig. 16 (a) and (b)), which results in more seismic energy being transferred

Table 5
Number of poundings at the left and middle expansion joints when the bridge structures are subjected to three different earthquake loadings.

	SMART1 earthquake	El-Centro earthquake	Simulated earthquake
Monolithic (left)	2	5	10
Segmental (left)	3	7	9
Monolithic (middle)	2	7	13
Segmental (middle)	3	10	11

to the bridge girders and leads to the more violent vibrations of bridge girders as discussed above. On the other hand, when the bridges are subjected to the simulated earthquake loading, the number of poundings in the monolithic bridge is, however, more than that in the bridge with segmental columns. This again can be explained by the hysteretic curves (Fig. 16(c)). It can be seen that under this earthquake loading, both bridge columns are almost in the elastic range, the bridge with monolithic columns are stiffer than that with segmental column as mentioned above, the stiffer structures are usually associated with more number of poundings because they vibrate faster as reported in many previous studies such as [15,41–43]. However, it is worth mentioning that this conclusion is drawn based on the condition that the response is linear elastic. When nonlinear inelastic response occurs, the response characteristics become more complex. Nonlinear inelastic response increases the displacement amplitudes, but vibration could at a different baseline as shown in Fig. 13. Moreover, the vibration frequency and phase also change with nonlinear responses. Therefore the observation on the number of poundings between adjacent elastic structures is not necessarily correct for nonlinear structures as demonstrated in the first two seismic excitations.

It should be noted that the above results are obtained from the bridge structures shown in Fig. 8, in which the vibration characteristics of the left and right bridge frames are the same. Pounding occurs only because of the displacement constraint by the abutments. The effect of frequency ratio on the seismic responses of the two adjacent bridge frames is discussed in Section 5.3.

5.3. Influence of frequency ratio

The influence of frequency ratio on the pounding responses of the bridge structures supported by monolithic columns have been extensively studied by many researchers (e.g. [15] and [16]). For the bridge structure supported by the segmental columns, no previous literature can be found. In this section, the influence of frequency ratio on the pounding responses between two segmental bridges is investigated. Besides the one discussed in Section 5.2, in which the frequency ratio between the left (f_1) and right bridge frame (f_2) is $f_1/f_2 = 1.0$, another two frequency ratios with $f_1/f_2 = 0.707$ and 1.414 are also studied in this section. The different frequency ratios are achieved by changing the mass of the right bridge frame shown in Fig. 1 to half and twice of the value in Section 5.2 respectively, while all the other parameters are kept the same as those in Section 5.2, i.e. the gap size is assumed as 0.1 m and poundings are considered. The pounding responses of the bridge structures subjected to the three different earthquake loadings shown in Fig. 11 are calculated. For conciseness, only the results obtained from the simulated earthquake loading is reported in this section. Moreover, for comparison, only the results of the left bridge frame are discussed.

Fig. 18 shows the influence of frequency ratio on the deck displacement time histories. It is interesting to note that when the frequencies of the two bridge frames are the same (i.e. $f_1/f_2 = 1.0$), the largest displacement response and the largest residual deformation are generated among the three cases. This is because when the vibration characteristics of the two adjacent bridge frames are the same, the two bridge frames tend to vibrate in phase, which means both bridge frames can vibrate more freely compared to the cases with different frequency ratios, therefore larger displacement is generated. The bridge frames are more likely to experience severer plastic deformations and thus result in larger residual displacement. To this end, the code specification that the vibration characteristics of the adjacent bridge structures should be close to unity in order to preclude pounding may not be a good choice because it may lead to larger displacement responses. Pounding inevitably damages bridge superstructure near the impacting areas, but restrains structure movement, hence reduces responses of bridge piers. As shown although the largest peak displacement is obtained when $f_1/f_2 = 1.0$, at other time instants, the bridge structures with different vibration characteristics generally experience larger displacements.

Fig. 19 shows the influence of frequency ratio on the impact force and Table 6 summarizes the numbers of poundings at the left and right expansion joints. As shown in Table 6, when the frequency ratio is unity, the least number of poundings occur at the middle expansion joint due to the in phase vibration. The number of poundings at the left expansion joint is almost the same for the three cases. This is because the left bridge frame is kept unchanged in these three cases and the differences mainly due to the poundings from the right bridge frame.

For the maximum pounding force, Fig. 19(b) shows that when $f_1/f_2 = 1.414$, it results in the largest pounding force and the smallest pounding force is obtained when $f_1/f_2 = 0.707$. This is because the larger mass of the right bridge frame results in the larger inertia resistance. The more severe pounding from the right bridge frame transfers more energy to the left bridge frame, which in turn leads to the slightly larger pounding force at the left expansion joint as shown in Fig. 19(a).

5.4. Influence of gap size

For the bridge with monolithic columns, previous studies show that the gap size can obviously influence the structural responses. For the bridge with segmental columns, no such previous studies were reported. This section investigates the influence of gap size on the seismic responses of bridge structure with segmental columns. For comparison, the corresponding results for the monolithic bridge are also plotted. In the numerical simulation, the vibration characteristics of the adjacent bridge frames are assumed to be the same in this section, while the gap size is increased from 5 cm with an interval of 5 cm to the size until the pounding between decks and at abutments is completely avoided. Again only the results of the left bridge frame obtained from the simulated earthquake loading are plotted and discussed.

Fig. 20(a) shows the peak deck displacements of the monolithic and segmental bridges with different gap sizes. As shown, the influence of column types on the peak deck displacement is not obvious, similar peak deck displacement can be obtained for all the considered gap sizes. Fig. 20(a) also shows that when the gap size is smaller than 0.2 m, bridge with segmental columns leads to larger peak deck displacement. However, when the gap size is larger than 0.2 m, bridge with monolithic columns has larger peak deck displacement. This might be because as shown in Fig. 20(b) when the gap is smaller than 0.2 m, both bridges deform mainly in the elastic range (relatively small residual displacements are observed as shown in Fig. 20(b)) because the adjacent bridge frames and abutments prevent large bridge displacement. When the gap size is larger than 0.2 m, the bridge with monolithic col-

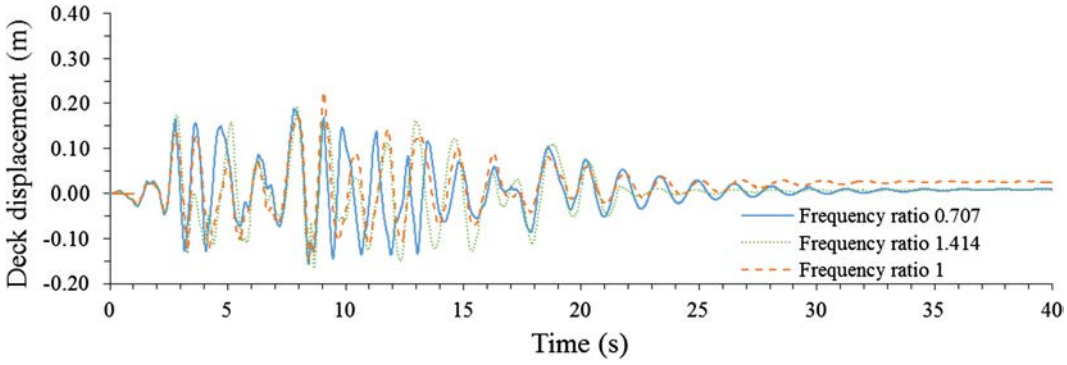

Fig. 18. Influence of frequency ratio on the deck displacement time histories of segmental bridge under artificially simulated earthquake.

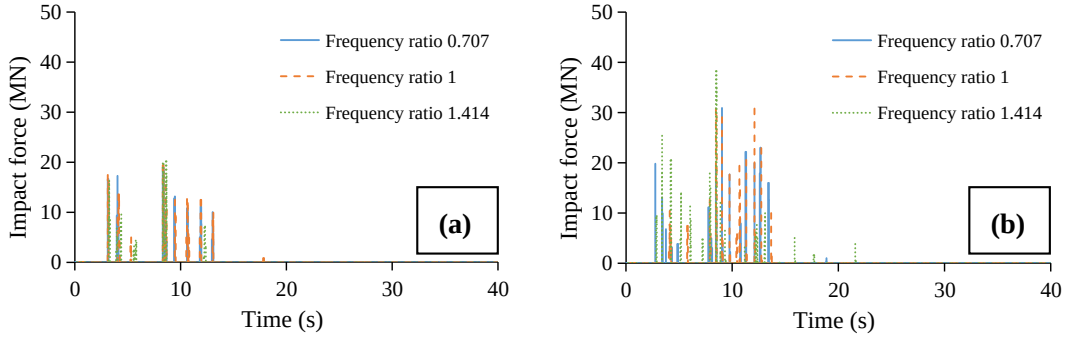

Fig. 19. Influence of frequency ratio on the impact force time histories. (a) Left expansion joint and (b) middle expansion joint.

Table 6
Influence of frequency ratio on number of poundings.

Frequency ratio	0.707	1	1.414
Left joint	8	9	7
Middle joint	15	11	16

umns experiences large plastic deformation (obvious residual displacement as shown in Fig. 20(b)). After the column is yield, the bridge deck cannot go back to the original position but oscillates around the yielding position at a smaller frequency. This results in larger peak displacement.

Fig. 20(b) shows the residual displacements of the two bridges with different gap sizes. As shown, when the gap size is smaller than 0.2 m, the vibrations of both bridges are restrained and they mainly deform in the elastic range. However, when gap size is large, the bridge structures can oscillate more freely. The large deformation leads to the monolithic bridge columns entering plastic range and results in larger residual displacement. For the bridge with segmental columns, the bridge columns can almost return to its original position due to the restoring force provided by the prestress tendons as mentioned above. In spite of the gap size, the bridge with segmental columns almost always has smaller residual displacement than the bridge with monolithic columns, demonstrating the advantages of using segmental columns in bridge constructions.

Fig. 21 shows the influence of gap size on the maximum pounding force at the left and middle expansion joints. As shown, at both expansion joints, bridge with monolithic columns almost always lead to the larger maximum pounding force. The figure also shows that larger gap size is required for the monolithic bridge to completely preclude pounding compared to the bridge with segmental columns. As shown in Fig. 21(a), at the left expansion joint, the required separation gaps are 0.45 and 0.4 m for the bridge with monolithic and segmental columns respectively, and at the middle expansion joint, the required values are 0.35 and 0.3 m respec-

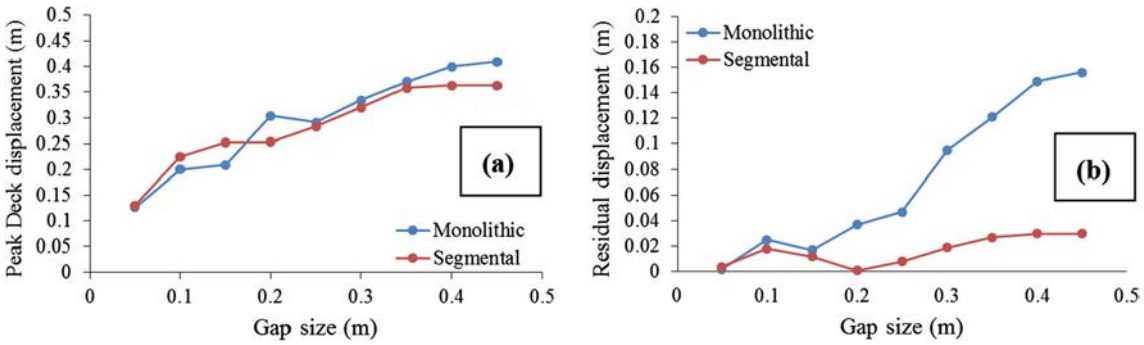

Fig. 20. Influence of gap size on the deck displacements. (a) Peak deck displacement and (b) residual displacement.

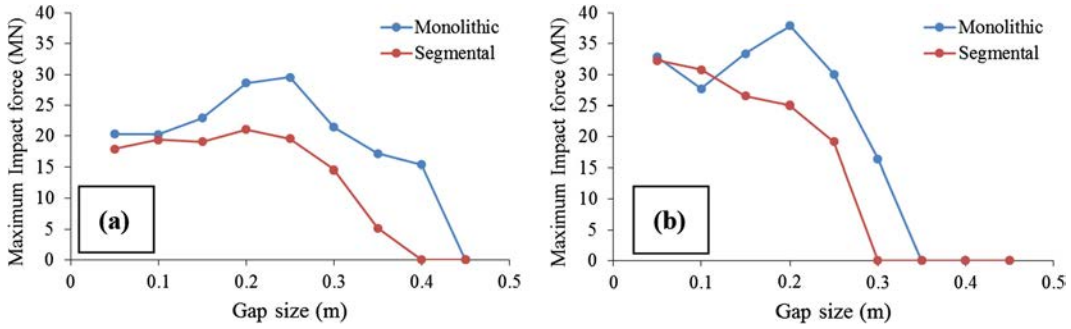

Fig. 21. Influence of gap size on the maximum pounding force. (a) Left expansion joint and (b) middle expansion joint.

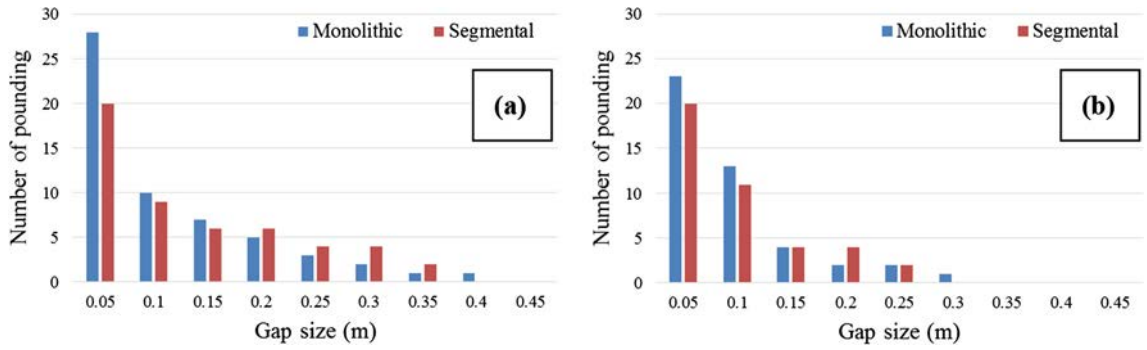

Fig. 22. Influence of gap size on the number of poundings. (a) Left expansion joint and (b) middle expansion joint.

tively. This is because large displacement is expected for the bridge with monolithic columns when plastic deformation occurs.

Fig. 22 shows the influence of gap size on the number of poundings for the bridges with monolithic and segmental columns. As shown when the gap size is smaller than 0.15 m, monolithic bridge results in more (or equal) number of poundings compared to the bridge with segmental columns. This is because as mentioned above, when the gap size is not big enough, both bridges deform almost within elastic range and the stiffer monolithic bridge leads to more number of poundings because of its higher vibration frequencies. When the gap size is larger than 0.15 m, the opposite trend is observed. This is because segmental columns dissipate less seismic energy and more violent super-structural vibrations are observed.

6. Conclusions

Bridge structures with precast segmental columns are more and more widely used in engineering practices. These bridge structures are normally located in the low seismicity areas due to the lack of understanding on their seismic performances. Recently, extensive research works have been carried out to examine the seismic performance of segmental columns. The investigations on the seismic responses of a whole bridge structure with segmental columns are rare. This paper carries out numerical studies on the seismic responses of bridge structure with precast segmental columns. For comparison, a similar bridge with conventional monolithic columns is also analyzed. The following conclusions are obtained based on the numerical results:

1. The bridge with segmental columns shows smaller residual displacement but more violent deck vibrations compared to the bridge with monolithic columns.
2. Pounding can reduce the bridge peak responses and residual displacement especially for the monolithic bridge.
3. Larger residual displacement can be generated when the vibration characteristics of the adjacent bridge frames are the same.
4. The influence of different gap sizes on peak displacement responses is similar to both bridges with monolithic and segmental columns. However, the influence of gap size on the residual displacement of the two bridges is different. For the monolithic bridge, larger gap size normally results in larger residual displacement. For the segmental bridge, the influence of gap size on the residual displacement is not prominent.
5. To completely preclude pounding, larger separation gap is required for the bridge with monolithic columns compared to the bridge with segmental columns.
6. When the gap size is small, bridge with monolithic columns experiences more number of poundings. When plastic deformation occurs, the bridge with segmental columns suffers more number of poundings.

Acknowledgement

The authors would like to acknowledge the following financial supports to carry out the research: the Australian Research Council Discovery Project DP150104346, the Major Research Plan of China National Railway Ministry of China under Grant No. 2015G003, the Research Plan of Sichuan Province, China under Grant No. 2015HH0058 and the scholarship from China Scholarship Council.

References

[1] Billington S, Barnes R, Breen J. Alternate substructure systems for standard highway bridges. J Bridge Eng 2001;6:87–94.
[2] Billington SL, Barnes RW, Breen JE. A precast segmental substructure system for standard bridges. PCI J 1999;44:56–73.

[3] Hewes JT, Priestley MN. Seismic design and performance of precast concrete segmental bridge columns. Report no. SSRP-2001/25, Univ. of California at San Diego. 2002.
[4] Chang KC, Loh CH, Chiu HS, Hwang JS, Cheng CB, Wang JC. Seismic behavior of precast segmental bridge columns and design methodology for applications in Taiwan. Taipei (Taiwan): Area National Expressway Engineering Bureau; 2002 [in Chinese].
[5] Ou YC, Chiewanichakorn M, Aref AJ, Lee GC. Seismic performance of segmental precast unbonded posttensioned concrete bridge columns. ASCE J Struct Eng 2007;133:1636–47.
[6] Chou CC, Chen YC. Cyclic tests of post-tensioned precast CFT segmental bridge columns with unbonded strands. Earthquake Eng Struct Dyn 2006;35:159–75.
[7] Marriott D, Pampanin S, Palermo A. Quasi-static and pseudo-dynamic testing of unbonded post-tensioned rocking bridge piers with external replaceable dissipaters. Earthquake Eng Struct Dyn 2009;38:331–54.
[8] ElGawady MA, Sha'lan A. Seismic behavior of self-centering precast segmental bridge bents. J Bridge Eng 2010;16:328–39.
[9] Motaref S, Saiidi MS, Sanders DH. Experimental study of precast bridge columns with built-in elastomer. Transport Res Rec: J Transport Res Board Bridge Eng 2010;3:109–16.
[10] Ou YC, Tsai MS, Chang KC, Lee GC. Cyclic behavior of precast segmental concrete bridge columns with high performance or conventional steel reinforcing bars as energy dissipation bars. Earthquake Eng Struct Dyn 2010;39:1181–98.
[11] Billington S, Yoon J. Cyclic response of unbonded posttensioned precast columns with ductile fiber-reinforced concrete. J Bridge Eng 2004;9:353–63.
[12] Motaref S. Seismic response of precast bridge columns with energy dissipating joints. Report no. CCEER-11-01, Univ. of Nevada at Reno; 2011.
[13] Zhang N. Dynamic properties and application of steel fiber reinforced self-consolidating concrete to segmental bridge columns in moderate-to-high seismic regions. PhD thesis, State Univ. of New York at Buffalo; 2014.
[14] Lee WK, Billington SL. Modeling residual displacements of concrete bridge columns under earthquake loads using fiber elements. J Bridge Eng 2009;15:240–9.
[15] Raheem SEA. Pounding mitigation and unseating prevention at expansion joints of isolated multi-span bridges. Eng Struct 2009;31:2345–56.
[16] Shrestha B, Hao H, Bi K. Effectiveness of using rubber bumper and restrainer on mitigating pounding and unseating damage of bridge structures subjected to spatially varying ground motions. Eng Struct 2014;79:195–210.
[17] Lowes LN, Mitra N, Altoontash A. A beam-column joint model for simulating the earthquake response of reinforced concrete frames. Report no. PEER 2003/10. Pacific Earthquake Engineering Research Center; 2004.
[18] Mitra N, Lowes LN. Evaluation, calibration, and verification of a reinforced concrete beam–column joint model. ASCE J Struct Eng 2007;133:105–20.
[19] McKenna F, Fenves GL, Scott MH. Open system for earthquake engineering simulation. Berkeley: University of California; 2004.
[20] Sideris P, Aref AJ, Filiatrault A. Large-scale seismic testing of a hybrid sliding-rocking posttensioned segmental bridge system. ASCE J Struct Eng 2014;140:04014025.
[21] Guo A, Li Z, Li H, Ou J. Experimental and analytical study on pounding reduction of base-isolated highway bridges using MR dampers. Earthquake Eng Struct Dyn 2009;38:1307–33.
[22] Li B, Bi K, Chouw N, Butterworth JW, Hao H. Experimental investigation of spatially varying effect of ground motions on bridge pounding. Earthquake Eng Struct Dyn 2012;41:1959–76.
[23] He L, Shrestha B, Hao H, Bi K, Ren W. Experimental and three-dimensional finite element method studies on pounding responses of bridge structures subjected to spatially varying ground motions. Adv Struct Eng. 2016:1369433216646009.
[24] Hao H, Bi K, Chouw N, Ren W. State-of-the-art review on seismic induced pounding response of bridge structures. J Earthquake Tsunami 2013;7:1350019.
[25] Shrestha B, Hao H, Bi K. Devices for protecting bridge superstructure from pounding and unseating damages: an overview. Struct Infrastruct Eng 2016:1–18.
[26] Megally S, Seible F, Garg M, Dowell RK. Seismic performance of precast segmental bridge superstructures with internally bonded prestressing tendons. PCI J 2002;47:40–57.
[27] Wang JC, Ou YC, Chang KC, Lee GC. Large-scale seismic tests of tall concrete bridge columns with precast segmental construction. Earthquake Eng Struct Dyn 2008;37:1449–65.
[28] Shen YL, Schneider J, Tesfamariam S, Stiemer SF, Mu ZG. Hysteresis behavior of bracket connection in cross-laminated-timber shear walls. Constr Build Mater 2013;48:980–91.
[29] Furtado A, Rodrigues H, Arêde A. Modelling of masonry infill walls participation in the seismic behaviour of RC buildings using OpenSees. Int J Adv Struct Eng 2015;7:117–27.
[30] Tirca L, Caprarelli C, Danila N, Calado L. Modelling and design of dissipative connections for brace to column joints. In: Dubina D, Grecea D, editors. 7th Int. workshop on connections in steel structures, Timisoara; 2012. p. 503–14.
[31] Taylor A, Kuo C, Wellenius K, Chung D. A summary of cyclic lateral load tests on rectangular reinforced concrete columns. Report no. NISTIR. 5984, National Institute of Standards and Technology; 1997.
[32] Mander JB, Priestley MJ, Park R. Theoretical stress-strain model for confined concrete. ASCE J Struct Eng 1988;114:1804–26.
[33] Filippou FC, Popov EP, Bertero VV. Effects of bond deterioration on hysteretic behavior of reinforced concrete joints. Report no. EERC 83–19. Berkeley: Earthquake Engineering Research Center, Univ. of California; 1983.
[34] Priestley MN, Seible F, Calvi GM. Seismic design and retrofit of bridges: John Wiley & Sons; 1996.
[35] Choi E. Seismic analysis and retrofit of Mid-America bridges. PhD thesis, Georgia Institute of Technology at Georgia; 2002.
[36] Zanardo G, Hao H, Modena C. Seismic response of multi-span simply supported bridges to a spatially varying earthquake ground motion. Earthquake Eng Struct Dyn 2002;31:1325–45.
[37] Chopra AK, McKenna F. Modeling viscous damping in nonlinear response history analysis of buildings for earthquake excitation. Earthquake Eng Struct Dyn. 2016;45:193–211.
[38] Center P. PEER Ground Motion Database. Pacific Earthquake Engineering Research Center, University of California, Berkeley, CA; 2013. http://ngawest2berkeley.edu.
[39] Zealand SN. Structural Design Actions: New Zealand. Earthquake Actions: Standards New Zealand; 2004.
[40] Li C, Hao H, Li H, Bi K. Theoretical modeling and numerical simulation of seismic motions at seafloor. Soil Dyn Earthquake Eng 2015;77:220–5.
[41] Chouw N, Hao H. Significance of SSI and nonuniform near-fault ground motions in bridge response I: Effect on response with conventional expansion joint. Eng Struct 2008;30:141–53.
[42] Chouw N, Hao H. Significance of SSI and non-uniform near-fault ground motions in bridge response II: Effect on response with modular expansion joint. Eng Struct 2008;30:154–62.
[43] DesRoches R, Muthukumar S. Effect of pounding and restrainers on seismic response of multiple-frame bridges. ASCE J Struct Eng 2002;128:860–9.